Contributed paper

OPTO-ELECTRONICS REVIEW **13**(3), 239–251

Growth and properties of MOCVD HgCdTe epilayers on GaAs substrates

P. MADEJCZYK[1], A. PIOTROWSKI[2], W. GAWRON[1], K. KŁOS[2], J. PAWLUCZYK[2], J. RUTKOWSKI[1], J. PIOTROWSKI[2], and A. ROGALSKI[*1]

[1]Institute of Applied Physics, Military University of Technology, 2 Kaliskiego Str., 00-908 Warsaw, Poland
[2]VIGO System S.A., 3 Świetlików Str., 01-389 Warsaw, Poland

Growth of MOCVD $Hg_{1-x}Cd_xTe$ (HgCdTe) epilayers on GaAs substrates is described. The paper focuses on the interdiffused multilayer process (IMP). In this process, the CdTe/HgTe growth times are comparable with transition times between the phases. The non-optimum flow velocities and partial pressures that may induce poor morphology and reduce growth rate characterize the growth during transition stages. The optimum conditions for the growth of single layers and complex multilayer heterostructures have been established.

One of the crucial stages of HgCdTe epitaxy is CdTe nucleation on GaAs substrate. Successful composite substrates have been obtained with suitable substrate preparation, liner and susceptor treatment, proper control of background fluxes and appropriate nucleation conditions. Due to the large mismatch between GaAs and CdTe, both (100) and (111) growth may occur. It mostly depends on substrate disorientation and preparation, nucleation conditions and growth temperature. Cd or Te substrate treatment just before growth results in (100) and (111) orientation, respectively. Generally, layers with orientation (100) show superior morphology compared to (111) but they are also characterized by hillocks.

The benefits of the precursors ethyl iodine (EI) and arsine (AsH_3) for controlled iodine donor doping and arsenic acceptor doping are summarized. Suitable growth conditions and post growth anneal is essential for stable and reproducible doping. In-situ anneal seems to be sufficient for iodine doping at any required level. In contrast, efficient As doping with near 100% activation requires ex-situ anneal at near saturated mercury vapours.

The transport properties of HgCdTe epilayers indicate on achieving device quality material. Reproducible n- and p-type doping at the low, intermediate and high level (10^{15}–10^{18} cm^{-3}) has been achieved with stable iodine and arsenic dopants. The mobilities and carrier lifetimes achieved for extrinsically doped n-type and p-type layers follow essentially the same trends observed in state-of-the-art liquid phase epitaxy grown HgCdTe.

Keywords: MOCVD growth, HgCdTe ternary alloy, carrier lifetime, transport properties.

1. Introduction

Historically, crystal growth of $Hg_{1-x}Cd_xTe$ (HgCdTe) has been a major problem mainly because a relatively high Hg pressure is present during growth, which makes it difficult to control the stoichiometry and composition of the grown material [1–4]. The wide separation between the liquidus and solidus, leading to marked segregation between CdTe and HgTe, was instrumental in the development of all the bulk growth techniques to this system. In addition to solidus-liquidus separation, high Hg partial pressures are also influential both during growth and post-growth heat treatments.

Early experiments and a significant fraction of early production were done using a quench-anneal or solid-state recrystalization process (Fig. 1). Bridgman growth was attempted for several years near the mid-70s last century. At the same time, solvent growth methods from Te-rich melts were initiated to reduce the grown temperature. One successful implementation was the travelling heater method (THM) up to 5-cm diameter [5]. The perfect quality of crystals grown by this method is occupied by a low growth rate.

The bulk HgCdTe crystals were initially used for any types of infrared photodetectors. At present they are still used for some infrared applications such as n-type single element photoconductors, SPRITE detectors, and linear ar-

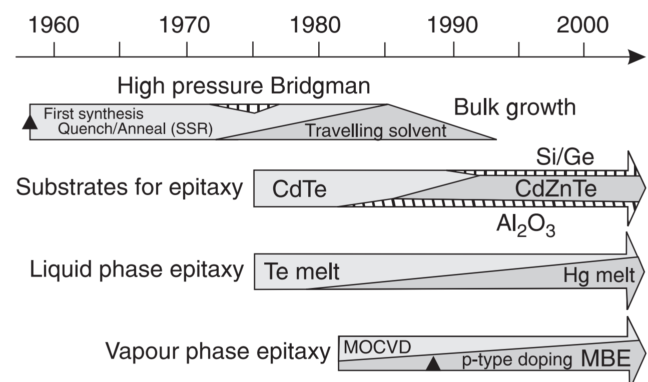

Fig. 1. Evolution of HgCdTe crystal growth technology from 1958 to present (after Ref. 4).

*e-mail: rogan@wat.edu.pl

rays. Bulk growth produced thin rods, generally to 15 mm in diameter, about 20 cm in length, and with non-uniform distribution of a composition. Large two-dimensional arrays could not be realized with bulk crystals. Another drawback to bulk material was the need to thin the bulk wafers, generally cut about 500 µm thick, down to final device thickness of about 10 µm. Also further fabrication stages (polishing the wafers, mounting them to suitable substrates, and polishing to the final device thickness) was labour intensive.

The epitaxial techniques offer, in comparison with bulk growth techniques, the possibility of growing large area epilayers and sophisticated device structures with good lateral homogeneity, abrupt and complex composition and doping profiles, which can be configured to improve the performance of photodetectors. The growth is performed at low temperatures, which makes it possible to reduce the native defects density. The properties of HgCdTe grown by the variety of techniques discussed here are summarized in Table 1.

Among the various epitaxial techniques, the liquid phase epitaxy (LPE) is the most matured method [6]. LPE is a single crystal growth process in which growth from a cooling solution occurs onto a substrate. LPE growth of thin layer on CdTe substrates began in the early-to-mid 70's. At present, the vapour phase epitaxy (VPE) growth of HgCdTe is typically done by nonequilibrium methods; metalorganic chemical vapour deposition (MOCVD) [7], molecular beam epitaxy (MBE) [8], and their derivatives. The great potential benefit of MBE and MOCVD over the equilibrium methods is the ability to modify the growth conditions dynamically during growth to tailor band gaps, add and remove dopants, prepare surfaces and interfaces, add passivations, perform anneals, and even grow on selected areas of a substrate. The growth control is exercised with great precision to obtain basic materials properties comparable to those routinely obtained from equilibrium growth.

In the case of MBE, a specially designed Hg-source ovens were successfully designed to overcome the low sticking coefficient of Hg at the growth temperature [8]. The growth temperature is less than 200°C for MBE but around 350–400°C for MOCVD, making it more difficult to control the p-type doping in the MOCVD due to formation of Hg vacancies at the higher growth temperatures. The vacancies can be removed by a low (<200°C) temperature anneal. However, in the case of MBE application, post growth annealing at high temperatures (above 350°C) is necessary for activation of acceptor dopant.

Earlier works on the fundamental issues of MOCVD growth and doping have been directed toward receiving of high quality cryogenically and thermoelectrically cooled HgCdTe photodiodes [7,9–11] and non-equilibrium devices [12,13]. This paper presents the recent advances in MOCVD of HgCdTe, with emphasis on these aspects of technology for the growth of heterostructure photovoltaic devices operated at room temperature in both middle wavelength (MW) and long wavelength infrared (LWIR) spectral ranges.

Table 1. Comparison of various methods used to grow HgCdTe.

	Bulk			Liquid phase epitaxy		Vapour phase epitaxy		
	SSR	THM						
		HCT melt	Te melt	Hg melt	Te melt	ISOVPE	MOCVD	MBE
Temperature (°C)	950	950	500	350-550	400-550	500	275-400	160-200
Pressure (Torr)	150 000	150 000	760-8000	760-11400	760-8000	760	300–760	10^{-3}-10^{-4}
Growth rate (µm/hr)	250	250	80	30-60	5-60	1-10	2-10	1-5
Dimensions w (cm)	0.8-1.2 dia	0.8-1.2 dia	2.5 dia	5	5	1 dia	7.5 dia	7.5 dia
l (cm)	–	–	–	6	5	–	4	4
t (cm)	15	15	15	0.0002-0.0030	0.0005-0.012	0.001	0.0005-0.001	0.0005-0.001
Density of dis. (cm^{-2})	$<10^5$	–	$<10^5$	$<10^5$	$<10^5$–10^7	–	5×10^5–10^7	$<5\times10^4$–10^6
Purity (cm^{-3})	$<5\times10^{14}$	$<5\times10^{14}$	$<5\times10^{14}$	$<5\times10^{14}$	$<5\times10^{14}$	$\approx1\times10^{15}$	$<1\times10^{15}$	$<1\times10^{15}$
n-type dop. (cm^{-3})	N/A	N/A	N/A	1×10^{14}-1×10^{18}	1×10^{15}-1×10^{16}	1×10^{15}	5×10^{14}-5×10^{18}	5×10^{14}-1×10^{19}
p-type dop. (cm^{-3})	N/A	N/A	N/A	1×10^{15}-1×10^{18}	1×10^{15}-5×10^{16}	1×10^{16}-5×10^{17}	3×10^{15}-5×10^{17}	1×10^{16}-5×10^{18}
X-ray r. c. (arc sec)	–	–	20–60	<20	<20	–	50–90	20–30
Uniformity (Δx)	<0.002	<0.004	<0.005	<0.002	<0.002	<0.001	±0.01-0.0005	±0.01-0.0006

 © 2005 COSiW SEP, Warsaw

2. MOCVD system

One of the important advantages of MOCVD system is the possibility of application of low-cost composite substrates (GaAs, Si, sapphire) as the viable alternative to costly CdZnTe substrates. This system does not require high vacuum for growth, is easier serviceable technique with larger throughput. Last, but not least, donor and acceptor doping at medium and high level, essential for near room temperature devices, is simpler with MOCVD. That is why we selected MOCVD as the technique of choice for fabrication of uncooled HgCdTe photodetectors.

Aixtron Aix-200 II-VI MOCVD system was purchased in 2004. Fast switching valves, high quality materials and proper reactor design allow us to run fully computer-controlled processes. Low to atmospheric pressure growth is possible. Drawback of this technique, in comparison with the previously used ISOVPE one [14–16], is high cost of equipment and high toxicity of precursors which is prevented by an advanced safety system.

Aixtron Aix-200 II-VI MOCVD system is a horizontal reactor customized for $Hg_{1-x}Cd_xTe$ growth on 2” wafers (Fig. 2). Pd-cell purified hydrogen is used as a carrier gas. Between processes the system is filled with nitrogen fined by getter purifier. Liquid nitrogen is used as the nitrogen source. Dimethylcadmium (DMCd), diisopropyltelluride (DIPTe), and diethylzinc (DEZn) used as precursors are held in temperature-stabilized baths. Elementary mercury is held in a quartz container in the lower input channel of the container. AsH_3 has been used as arsenic precursor. The drawback of arsine is its toxicity. Special safety preventive measures must have been applied to the laboratory.

Ethyl iodide (EI) is used for donor doping. Because of its high vapour pressures, the metalorganic source for iodine must be held at low temperatures (<5°C).

DMCd/EI and DIPTe/AsH_3 input channels are separated to prevent premature gas mixing and dust formation. Evaporating mercury is carried by hydrogen to the growth zone. Drawback of this solution is the dissolution of Te and As sources in the elementary mercury container. This may result in As memory effects. The surface of the mercury is covered with black skin, probably HgTe after deposition causing growth instabilities.

Hydrogen from the upper channel dilutes mercury saturated hydrogen from the lower channel. Therefore decrease in the mercury partial pressure over the wafer must be taken into account and it can be altered by changing the lower to upper channel flow ratio. In practice, the flow is selected separately for each phase; for example 100/500 sccm or 1200/1200 sccm flow ratios have been used. In this notation the first number is mass gas flow in the upper channel and the former is mass gas flow in the lower channel.

Two temperature zones are in the reactor: the mercury source zone (up to 300°C) and the growth zone with graphite susceptor (up to 900°C). Reactor temperatures 360–410°C have been used and mercury has been held in 200–220°C. Higher temperatures are used for reactor cleaning.

Substrate is lying on a rotating disk using Aixtron’s gas foil rotation technique. Vacuum system provides the possibilities of keeping the reactor at the pressures from 50 mbar to atmospheric pressure. Reactor pressure of 500 mbar was used for all successful growth runs.

MOCVD system contains explosive materials such as hydrogen and toxic materials as AsH_3, mercury and metalorganics precursors. Therefore the laboratory is equipped with advanced safety feature devices such as hydrogen, arsine and mercury detectors, effective ventilation system, and different safety interlocks embedded in the Aixtron’s system. Large quantities of mercury are being transported during the growth. They are condensed at low temperature

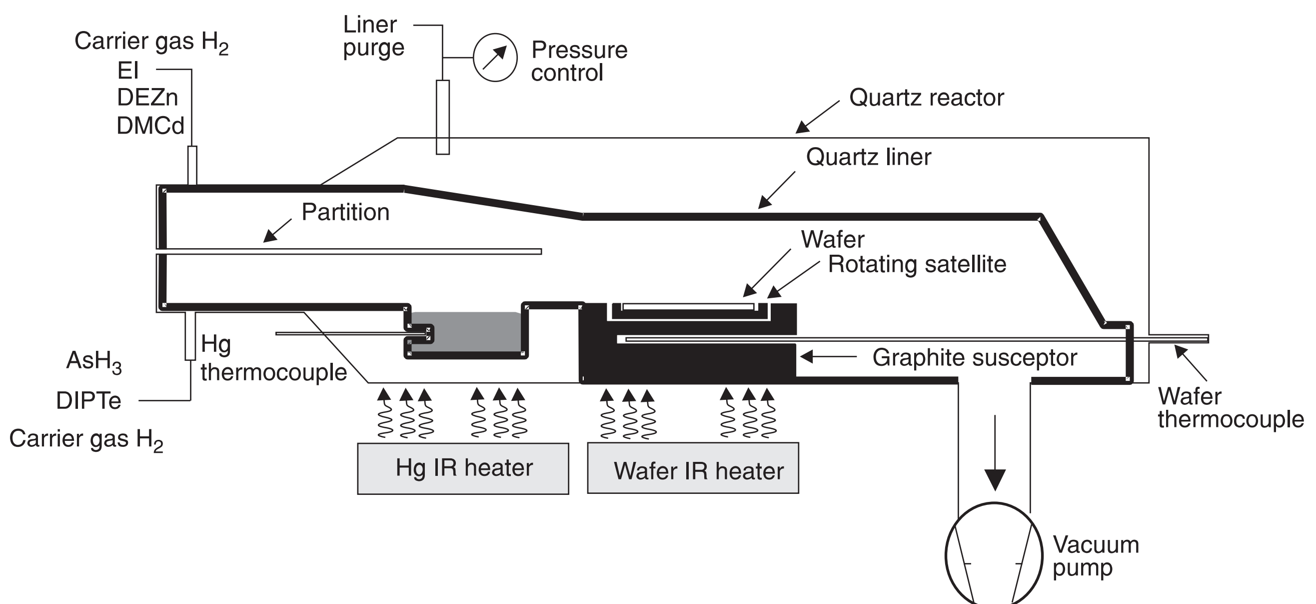

Fig. 2. Schematic drawing of Aix-200 II-VI reactor.

Hg trap. Glovebox nitrogen atmosphere contains a lot of mercury and all its gas outlets are equipped with activated coal filters. All toxic gases are neutralized in the wet scrubber system.

3. $Hg_{1-x}Cd_xTe$ growth

CdTe buffer growth on GaAs is probably the most critical stage in HgCdTe growth due to lattice mismatch. For GaAs and CdTe, the mismatch is approximately 14.3%. 2–10-μm thick CdTe buffer neutralizes so huge mismatch. The buffer plays also a role of Ga diffusion barrier [17].

Careful chemical and thermal treatment of the reactor must be carried out after each growth run to prevent residual deposits of HgCdTe on substrate that adversely affect nucleation stage of growth. Different phases on the edges and in the middle of the wafer were frequently observed for poorly cleaned reactor.

Epiready (100) GaAs wafers with 2–4° disorientation towards <100> and <110> have been used. Due to the large mismatch between GaAs and CdTe, both (100) and (111) growth may occur. It mostly depends on substrate disorientation and preparation, nucleation conditions and growth temperature. Cd or Te substrate treatment just before growth results in (100) and (111) orientation, respectively.

Generally, layers with orientation (100) show superior morphology compared to (111) but they are also characterized by hillocks. Height of hillocks is typically twice higher compared to the layer thickness.

Origin of hillocks is not fully understood at present. Hillocks are created during CdTe buffer growth and HgCdTe growth only enlarging them. Epilayers with hillocks are practically useless for device fabrication. Various ways to prevent hillocks formation have been tried: Zinc nucleation layer, different Cd/Te ratios, different substrates orientations have been used, but we were able to grow hillocks-free layers only on some substrates from one supplier (Fig. 3). Therefore, most of the devices were based on (111) layers.

Direct $Hg_{1-x}Cd_xTe$ growth is difficult due to different thermodynamic properties of HgTe and CdTe [7,18]. We applied interdiffused multilayer process (IMP) for $Hg_{1-x}Cd_xTe$ growth to avoid this problem. IMP gives the possibility for controllable growth of heterostructures with complex composition and doping profiles. HgTe and CdTe layers are deposited one after another with the period 100–200 nm and homogenized by interdiffusion during growth. Any composition can be achieved this way by proper selection of HgTe and CdTe layer growth times.

IMP growth depends in a complex way on precursors concentration, flow velocities, growth temperature and many other factors, frequently dependent on the reactor design. A lot of optimization is required to obtain good quality layers.

One of the critical factors is a proper control of precursors delivery to the growth zone. For practical devices we need multilayer heterostructures with uniform lateral composition and doping level within each layer and, at the same time, with sharp interfaces. This implies very thin IMP pairs and quite short times of CdTe and HgTe growth phases. The practical consequence is that IMP times become comparable to the times required for precursor transport from bubblers to the growth zone. The other complications are significant differences in the transport times for different precursors, mixing effects and different carrier gas flow velocities for the CdTe and HgTe growth stages [7]. This may result in poor control of the actual concentration of precursors that could adversely affect the quality, homogeneity and doping of the HgCdTe layers. Reduction of precursor's delivery times is possible with increased carrier gas flow but the shorten residence time of precursors decreases pyrolysis efficiency, which leads to the waste of expensive metalorganic precursors.

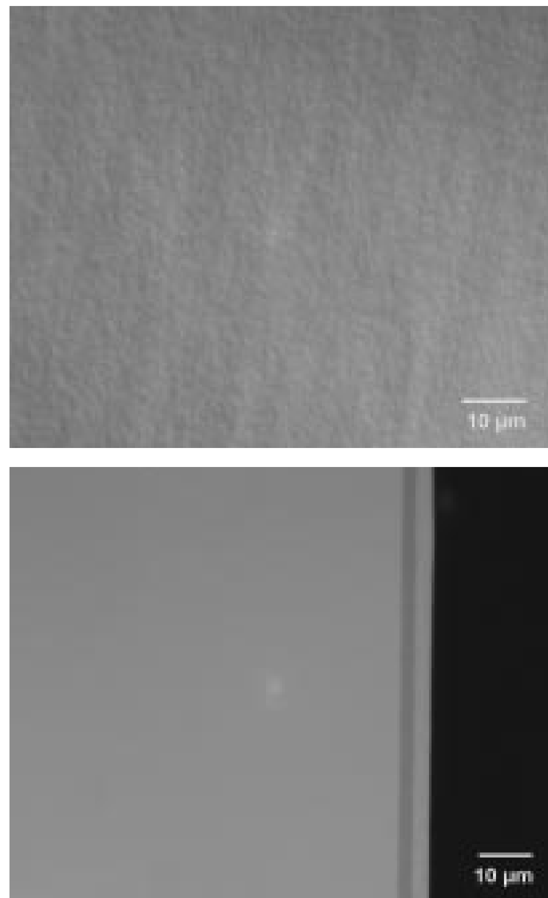

Fig. 3. Surface morphology and cleavage of (100) layer.

The problems described above can be solved to some degree by the use of four-phase IMP process proposed by Svoronos *et al*. [19]. The carrier gas flow through DIPTe bubbler is switched on at the start of HgTe phase and switched off at the beginning of HgTe flush phase. DIPTe and DMCd bubblers are switched on and off at the start and at the end of CdTe phase, respectively. Typically, the carrier gas flow during CdTe/CdTe flush phase is approximately 4 times longer of that during the HgTe/HgTe flush one [20]. The CdTe phase is usually used also to introduce

 © 2005 COSiW SEP, Warsaw

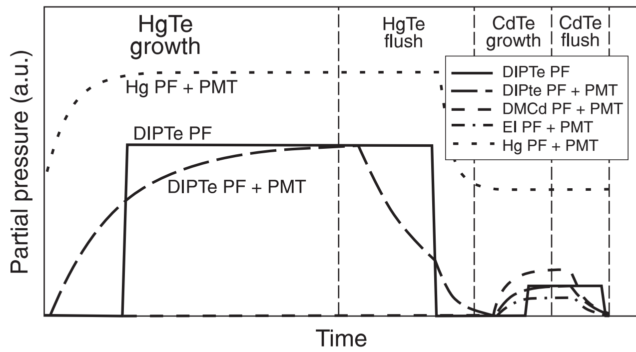

Fig. 4. Modelling precursor concentration during IMP technique. DMCd and DIPTe in scale, Hg scale ×17, EI scale ×200. We assume equal delays for all precursors in CdTe growth phase.

doping precursors. CdTe growth phase is critical for growth of low composition MCT because of its shortness.

Careful selection of the flows and valve switching times is necessary to ensure optimum growth conditions. Experimental optimization of the growth conditions is costly and time consuming. The theoretical modelling has been used as the first approximation that could be eventually corrected with suitable experiments. Figure 4 shows modelled partial pressures of precursors in growth zone during four-stage IMP. The most simple approximation is the plug flow (PF) model that describes temporal changes of precursor concentration as rectangular pulses characterized by delays compared to the nominal HgTe and CdTe phases (Fig. 4 – DIPTe PF). This means that the HgTe and CdTe growth occurs partially during the HgTe and CdTe phases, and partially are continued during the flush phases.

The PF model is usually a good approximation of gas flow through a thin pipe but poor for the liner volumes of complex shape, where mixing effects are significant. The mixing effects and changes of carrier gas flow may cause significant distortion of the pulses (Fig. 4). The distortion depends on the design of particular gas system and differs for various precursors.

HgTe growth phase

Low carrier gas total flow velocity causes large delay of DIPTe precursor. Time needed for precursor to pass through the pipes from bubbler to reactor is estimated with PF model (DIPTe PF – Fig. 4).

HgTe flush phase

Total flow rate is changed during that phase. Increase in total gas flow rate during CdTe phase could cause unstable growth conditions because of changing partial pressure of DMCd and DIPTe at the beginning of CdTe deposition. Time of the flush after HgTe is a compromise. From one hand it must be carefully selected to ensure no residual DIPTe precursor pressure during the CdTe growth phase. On the other hand it must be short enough to avoid evaporation of HgTe. Low residual DIPTe partial pressure after the flush phase is particularly important for doping, where DMCd/DIPTe ratio must be precisely controlled.

CdTe growth

CdTe layers deposited during IMP cycle must interdiffuse during next a few cycles to ensure composition uniformity. Injected precursors have different delivery times, so they can't be switched on simultaneously. Delays and bad switching moments can cause deterioration of morphology [especially (100) one], inefficient doping, and unintentional direct growth.

CdTe flush

CdTe flush phase is less critical for growth, because of low evaporation velocity of CdTe.

In practice, the partial pressures of precursors could be predicted with limited accuracy and the process' design has to be experimentally adjusted. Doping and flushes times are longer than modelling results pointing at. In reality, during IMP the precursors switching are much more complicated. Properties of mass flow controllers forced us to use delta doping to achieve low-doped MCT layers. CdTe growth time is kept constant in all absorber layers. We observed large, nonlinear, composition shifts when we change CdTe growth time; therefore the composition calibration was adjusted through HgTe growth time.

Linear deposition characteristics over substrate must be assured to avoid non-uniformity of HgCdTe composition. First of all, deposition characteristics depend on linear flow velocity over substrate.

The composition uniformity across the wafer has been evaluated by mapping of infrared transmission spectra. The transmission spectra are close to the theoretical ones. This is an evidence of good in-depth homogeneity. The composition uniformity over the wafer as low as ±0.1% is achieved.

4. Undoped $Hg_{1-x}Cd_xTe$ layers

Electrical properties of nominally undoped $Hg_{1-x}Cd_xTe$ layer are determined by native acceptors (metal vacancies) and uncontrolled background doping. Vacancy concentration strongly depends on reactor temperature, vapour pressure and material composition. The native doping level after growth at 360°C with mercury temperature 200°C is approximately 5×10^{16} cm^{-3}. This is much below the expected level of $>1\times10^{17}$ cm^{-3} for this temperature conditions [21]. We suspect that it is due to partial annihilation of vacancies during cool down. It could be influenced by hydrogen presence in the layer.

Post-growth annealing in mercury vapours can change the vacancy concentration. Vacancies may be practically eliminated by a prolonged, low temperature (≈200°C) annealing at near saturated mercury pressures. Such annealing reveals the background doping level. We have observed the uncontrolled background about $N_d - N_a = (1–3)\times10^{15}$ cm^{-3} for our MOCVD system.

Ex-situ anneal in sealed quartz ampoules in mercury vapours is typically used to maintain isothermal conditions. This technique is not practical for production purposes. Instead, we developed more convenient *ex-situ* anneal technique in which a wafer after growth was transported into reusable quartz container. Temperatures up to 400°C and Hg pressures up to 2 bars could be used.

High and low temperature annealing was used. Typically, a short (approx. 20 min–3 h) high temperature (360°C) anneal was used for doping homogenization followed by long (>2 h) low temperature (250°C) anneal for vacancy annihilation. Mercury pressure has been changed during both stages of this annealing to maintain conditions close to isothermal ones.

In-situ annealing is very practical for production purposes. It is carried out in the reactor immediately after the growth. The annealing eliminates the need for any "hot" processes after removal of wafers from the MOCVD reactor, and the possibility of additional impurities introduction.

When the growth is finished, the temperature of the wafer is gradually lowered to 210°C for 1–6 hours keeping the mercury source temperature at the 200–220°C. After that both reactor and mercury are cooled down. It must be avoided to cool down the rector below the mercury level to prevent Hg droplet formation. During annealing it is not possible to close the reactor and to stop hydrogen flow. This result in significant mercury losses. In practice, this means that we cannot obtain near saturated mercury pressures at temperatures >220°C. This effect can be limited by selecting optimal upper to lower channel flow ratio.

Vacancy and background doping is not sufficient for advanced infrared devices that require donor and acceptor doping at medium and high doping levels.

5. $Hg_{1-x}Cd_xTe$ doping with foreign impurities

Iodine and arsenic have been used as foreign dopants. Both are well behaved, stable and slowly diffusing dopants. To be active dopants they must occupy Te sites. Metal-rich conditions are favourable for iodine incorporation and they are required for arsine. Therefore they have been introduced during CdTe phase with Cd/Te ratio >1. Most of doping experiments have been carried out for (111) $Hg_{1-x}Cd_xTe$ layers.

Layer characterization techniques included room-temperature infrared transmission to determine composition x and layer thickness, Hall measurements at 2 kG magnetic field to determine electrical carrier concentration and mobility, and secondary ion mass spectroscopy (SIMS) to determine dopant concentrations. Profiling of the layers was achieved by differential Hall assessment using etch-step removal on samples with protected contacts. Additionally, the compositional profiles were evaluated for some samples by differential reflection spectra. The electrical measurements were carried just after growth (*in-situ*) and after postgrowth annealing of the layers under Hg-saturated conditions (typically 360°C/3h and 250C/5h) to remove Hg vacancies. After such annealing, undoped layers typically showed mixed conduction at 77 K or were lightly p-type with carrier concentrations less than 5×10^{15} cm^{-3}, due to residual background impurities. In some cases samples were previously annealed at 400°C for 10 h under Te-rich phase equilibria (Hg held at 250°C in a two-zone furnace) to check the stability of dopant site occupation under conditions of excess Hg vacancy concentration.

The carrier lifetime was measured using the steady-state photoconductivity technique. The sample is illuminated with a modulated calibrated flux and lock-in technique is used. The minority carrier lifetime is determined provided the quantum efficiency, the flux, and the mobilities are known. Lifetime characterization has been also performed by interpretation of exponential photoconductivity decay using a pulsed laser.

5.1. Iodine doping

Iodine is well behaved dopant and it is typically used to obtain heavily doped n^+-layers. It is a highly effective precursor without any memory effects [22]. Therefore it is important to establish conditions for iodine doping at $>10^{17}$ cm^{-3} level. Cd/Te ratio of 1.1–1.3 has been used during CdTe phase to improve efficiency of I incorporation and activation. It allows doping concentration between 1×10^{17} and 1×10^{18} cm^{-3} for the compositions of about 0.3.

It appears that iodine incorporation efficiency in HgCdTe from EI exhibits a strong dependence on the precise orientation of the substrate [23]. Figure 5 shows the concentration of iodine in $Hg_{1-x}Cd_xTe$ ($x \approx 0.20$) layers, measured by SIMS, for a number of misorientations from the (100) plane toward (111)B. During growth, the EI partial pressure was maintained at constant values marked in the figure. The HgCdTe layers were grown on CdZnTe [23] and GaAs substrates (our results). We can see that the iodine concentration varies over a wide range form mid-10^{15} cm^{-3} for (100)8°→(111)A to mid-10^{18} cm^{-3} for the (211)B orientation. The variation in dopant incorporation with crystallographic orientation is well known for several dopants in GaAs and other III-V semiconductors. The iodine occupies the Te sublattice sites substitutionally. The Te sides on the (211)B surface provide a more stable and favourable adsorption site with three bonds from the underlying group II atoms while the (100) surface provides a weaker adsorption site with two bonds.

Next figure (Fig. 6) shows the efficiency of iodine doping as a function of EI partial pressure for two orientations of HgCdTe layers. The growth conditions for both orientations were identical. We observe significantly higher incorporation rates in the (111) orientation. For comparison, the solid trend-lines are taken from Ref. 9 for (211)B and (100)4°→(110) orientations.

Multi-level staircase structure quickly yielded dopant source calibration curves. Figure 7 shows calibration structure obtained using ethyliodide (EI) which was assessed by SIMS measurements and differential 77 K Hall profiling.

 © 2005 COSiW SEP, Warsaw

The errors in differential Hall concentrations become larger when the etch step sizes are reduced and the minimum reliable step is around 2 µm. Consequently, it is difficult to align the step positions with the grown layer interfaces.

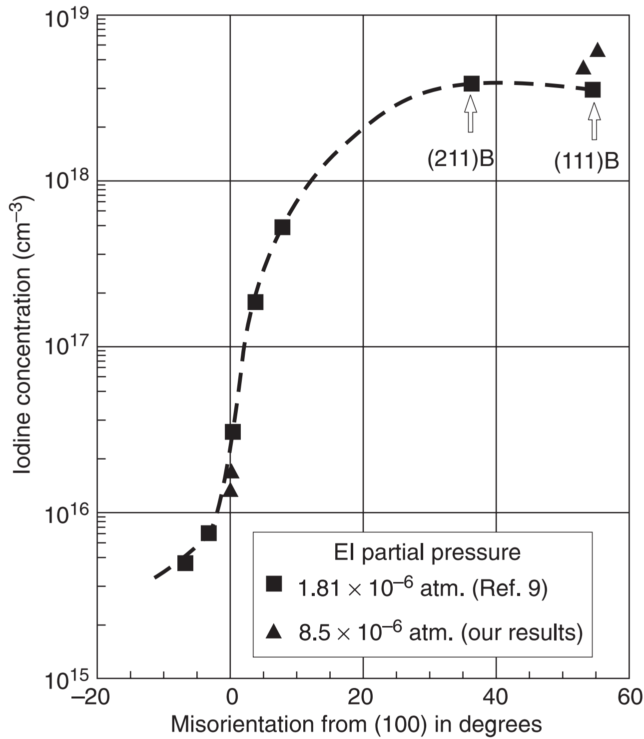

Fig. 5. Iodine incorporation in $Hg_{1-x}Cd_xTe$ ($x \approx 0.20$) vs. misorientation from the (100) plane toward (111)B measured by SIMS. During growth, the EI partial pressure was maintained at constant values: 1.81×10^{-6} atm. (■, after Ref. 9) and 8.5×10^{-6} atm (▲, our results).

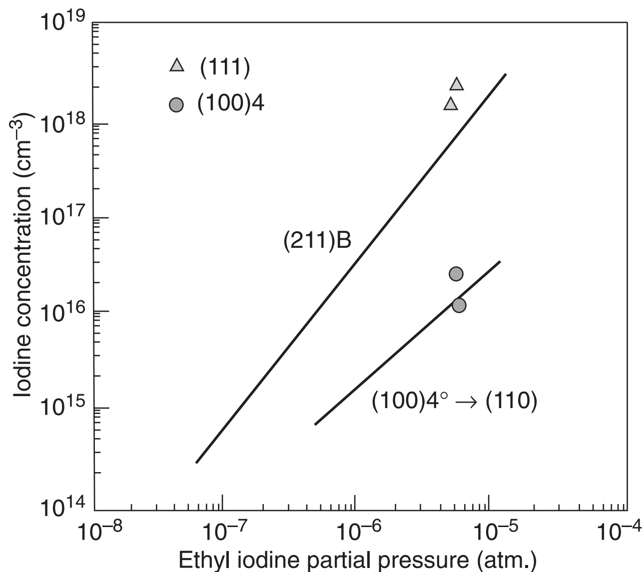

Fig. 6. Iodine incorporation in $Hg_{1-x}Cd_xTe$ ($x \approx 0.20$) as a function of EI partial pressure for (100) and (111) orientation. The solid trend-lines are taken from Ref. 9 for (211)B and (100)4°→(110) orientations.

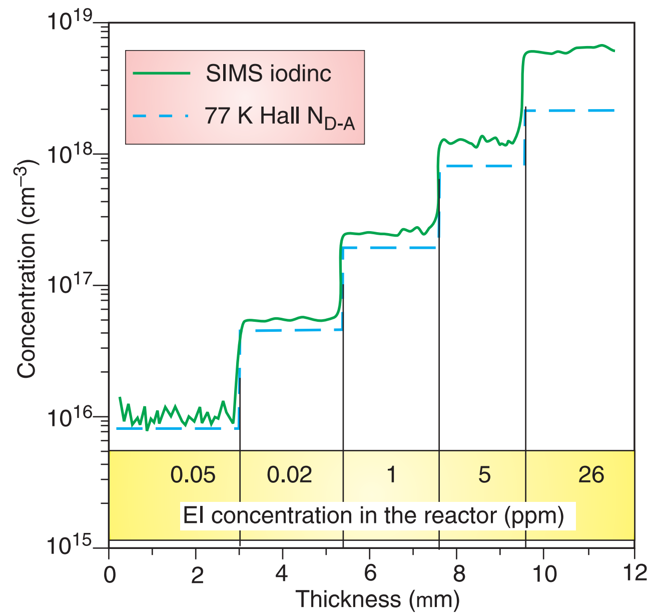

Fig. 7. Calibration profile of staircase $(111)Hg_{0.66}Cd_{0.34}Te$ structure doped using ethyliodide. I-doped HgCdTe structure was grown with Cd/Te ratio of 1.2.

The obtained correlation between the electrical and chemical results implied the iodine incorporated on the correct Te lattice site; and that within the accuracy of the techniques, the activation efficiency is close to 100%. However, along with increasing iodine concentration its activation decreases. Probably for high iodine concentration it starts to occupy interstitials or metal sites. Although EI shows the desirable properties of a donor dopant source, the minimum EI concentration about 0.2 ppm could be obtained with sensible choices of source temperature and double dilution mass flow controllers (MFC) settings. The range of 0.05 ppm (first step at calibration structure) was obtained by setting very short injection times to the reactor – 0.4 sec of EI. The control of iodine concentration is difficult below 1×10^{16} cm^{-3}.

Good reproducibility of I doping has been observed. Also no or insignificant I doping memory effects have been observed. Figure 8 shows the relationship between 300 K electron concentration and alloy composition. It is clearly shown decrease in iodine incorporation with composition increasing. Preliminary experiments with increasing Cd/Te ratio have not improved EI doping noticeably. However, slight improved efficiency of doping has been observed with *ex-situ* annealing at 360°C at near saturated mercury pressures. This effect may be related to incomplete iodine homogenization during growth and *in-situ* annealing, since iodine diffusion is very slow (noticeably slower then Cd diffusion into HgTe).

Heterostructure photovolataic IR detectors require heavily doped n^+-layers with relatively high x composition ($x > 0.45$). It is expected that such layers should have resistivity as small as possible to provide good electrical con-

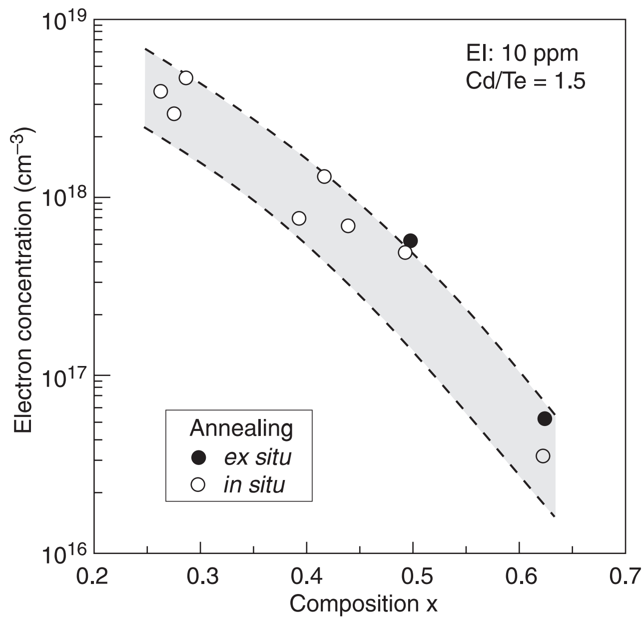

Fig. 8. Room temperature electron concentration for iodine doped HgCdTe layers vs composition x. HgCdTe layers were grown with Cd/Te ratio of 1.5.

tact. Until now, the $Hg_{1-x}Cd_xTe$ layers with composition $x > 0.45$ doped with EI doses above 10 ppm had electron concentration lower than 7×10^{17} cm^{-3} and sheet resistance above 10 Ω. These parameters indicate that significant part of iodine atoms are not located in Te lattice and are not electrically active.

The transport properties of iodine-doped HgCdTe layers have been also characterized extensively in our laboratory. In Fig. 9, the 77 K mobilities obtained as a function of electron concentration for iodine-doped samples are shown. We note that the mobilities of electrons in samples fabricated in our laboratory are comparable with previously published values for layers doped using iodine as a vapour from the solid element [24]. Expected decrease in mobility with increasing doping is due to ionized impurity scattering mechanism.

Temperature-dependent lifetime measurements have been carried out using the steady-state photoconductivity technique. For example, the data for $Hg_{0.68}Cd_{0.32}Te$ samples with electron concentrations 1.1×10^{16} cm^{-3} and 2.0×10^{16} cm^{-3} are shown in Fig. 10. Both sets of data agree well with a theoretical model that includes Auger 1 and radiative recombination mechanisms [3].

The next figure (Fig. 11) shows the 77 K lifetimes for n-type doped $Hg_{0.77}Cd_{0.23}Te$ layers against electron concentration. The layers have been doped using triisopropyl indium and ethyliodide. The trend-line follows the expected $1/n_i^2$ dependence for Auger limited lifetime, increasing to > 1 μs at 10^{15} cm^{-3}.

5.2. Arsenic doping

For acceptor doping, the most widely used dopant in HgCdTe is arsenic. In MOCVD there have been extensive studies of arsenic doping with a variety of precursors. The most popular is arsine (AsH_3) used also in our laboratory. As less toxic liquid precursors such as tertiarybutylarsine ($TBAsH_2$), phenylarsine ($PhAsH_2$) and dimetyhylamino-arsenic (DMAAs) became commercially available.

Arsine incorporation into Te sites is very sensitive for metallic rich conditions. This assures conditions for arsenic to enter Te sites where it acts like an acceptor. Otherwise arsenic can show amphoteric behaviour.

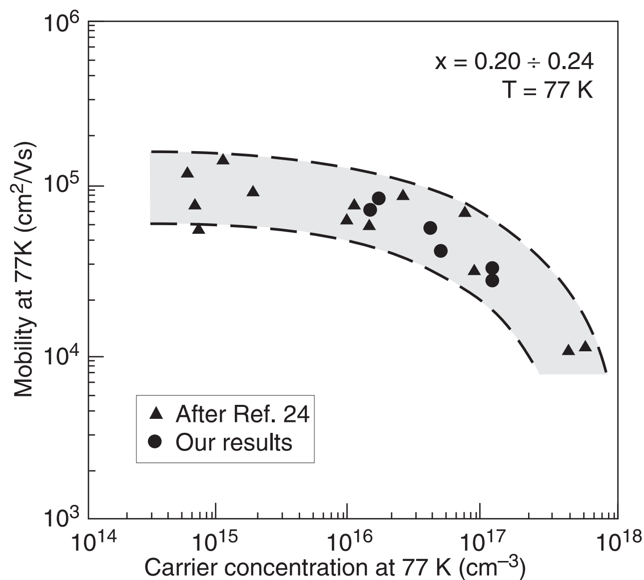

Fig. 9. 77 K mobilities of iodine doped $Hg_{1-x}Cd_xTe$ ($x = 0.20$–0.24) layers vs. electron concentration. The layers have been doped using etyliodine (●) and iodine as a vapour from the solid element (▲, after Ref. 24).

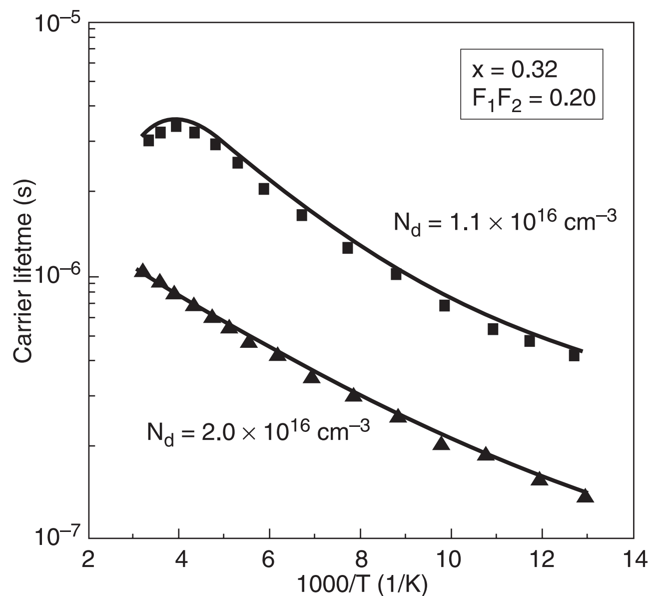

Fig. 10. Temperature dependence of lifetimes measured for $Hg_{0.68}Cd_{0.32}Te$ samples with electron concentrations 1.1×10^{16} cm^{-3} and 2.0×10^{16} cm^{-3} and comparison to the theoretical model (solid lines).

 © 2005 COSiW SEP, Warsaw

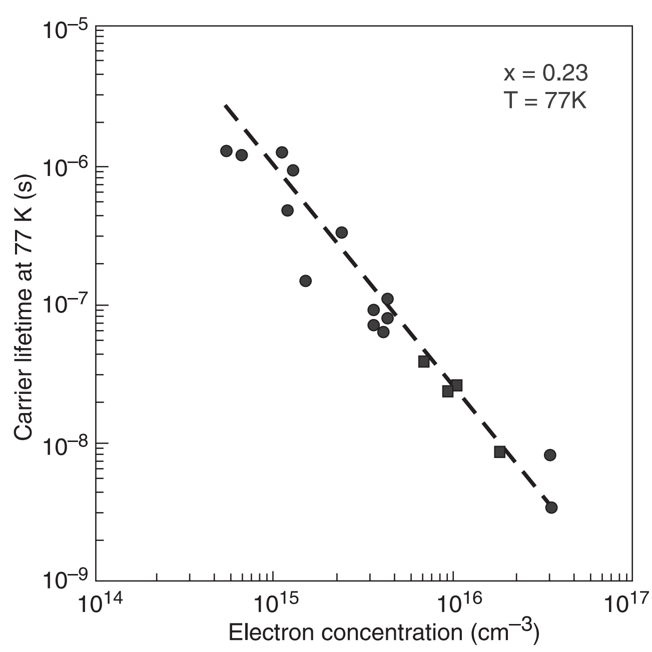

Fig. 11. 77 K carrier lifetime as a function of electron concentration for $Hg_{0.77}Cd_{0.23}Te$ layers. The layers have been doped using triisopropyl indium (●, after Ref. 26) and ethyliodide (■, our results).

The arsenic incorporation rate and doping efficiency strongly depend on crystallographic orientation. Figure 12 shows the efficiency of arsenic doping as a function of AsH_3 partial pressure for two crystallographic orientations: for the (100) and (111). Different orientations were obtained by different nucleation conditions. The difference in doping efficiency for two orientations is clearly evident, with near an order of magnitude higher incorporation rate

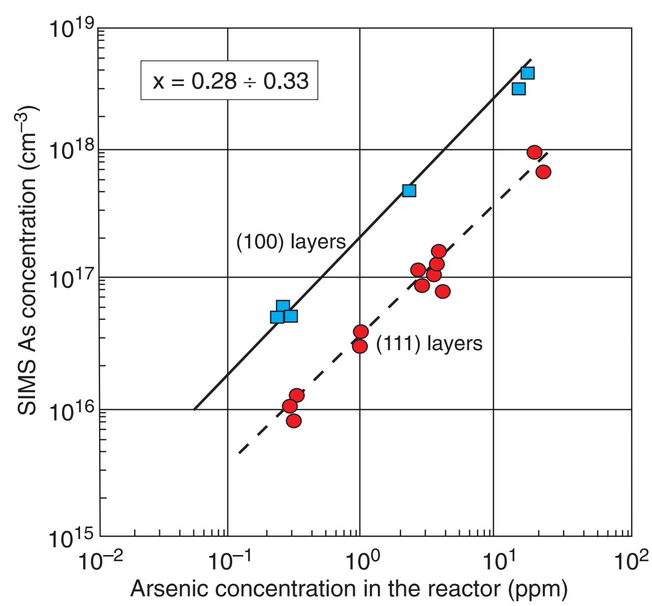

Fig. 12. Arsenic incorporation in $Hg_{1-x}Cd_xTe$ (x = 0.28–0.33) vs. AsH_3 partial pressure, measured by SIMS for the (100) and (111) orientations.

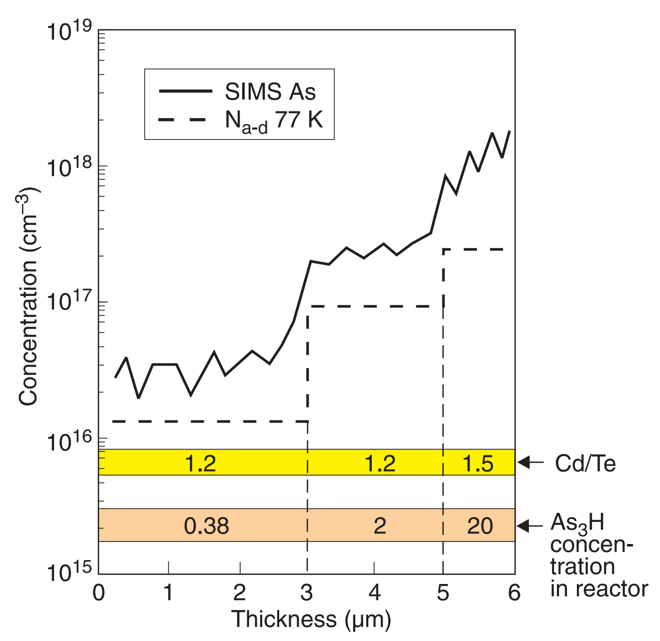

Fig. 13. Calibration profile of staircase $(111)Hg_{0.68}Cd_{0.32}Te$ structure doped using arsine: A – 2 ppm AsH_3 dose was introduced during 3 sec of 16-sec length of time CdTe cycle; B – 2 ppm AsH_3 dose was introduced during both cycles of IMP growth; C – 20 ppm AsH_3 dose was introduced during both cycles of IMP growth. As-doped HgCdTe structure was grown with Cd/Te ratio of 1.2–1.5.

in (100) orientation. This strong polarity dependence can be qualitatively understood by considering that the two Cd and As atoms are jointly involved in the incorporation process, because the adsorbed species originate from the adduct DMCd-AsH_3. The detailed explanation of this phenomenon is presented in Ref. 25.

To assess a doping source and to reduce the number of growth experiments, the test doping structures have been prepared. Multi-level "staircase" structures quickly yielded dopant source calibration curves. Figure 13 shows a "staircase" structure obtained using AsH_3 which was assessed by SIMS and differential 77 K Hall profiling. The SIMS data are referenced to the growth interface and plotted as a function of layer thickness. The correlation obtained between the chemical and electrical results implied the arsenic incorporated on the correct Te lattice site. However, comparing Figs. 7 and 13, we can notice less activation efficiency for arsenic than for iodine. In general, the activation energy is almost 100% in low concentration range and decreases with increasing arsenic incorporation in (111) HgCdTe layers. In our AsH_3 gas system it is difficult to introduce doses lower than 2 ppm. To obtain acceptor concentration of about 10^{16} cm^{-3}, what corresponds arsine fraction of 0.38 ppm, the doses of 2 ppm have been introduced in the growth zone during 3 sec of 16-sec length of time CdTe cycle.

Next figure (Fig. 14) shows the result of a three-layer structure grown with AsH_3 to check memory effects. In this structure, at the first interface the AsH_3 concentration was switched on, and at the second interface – was switched

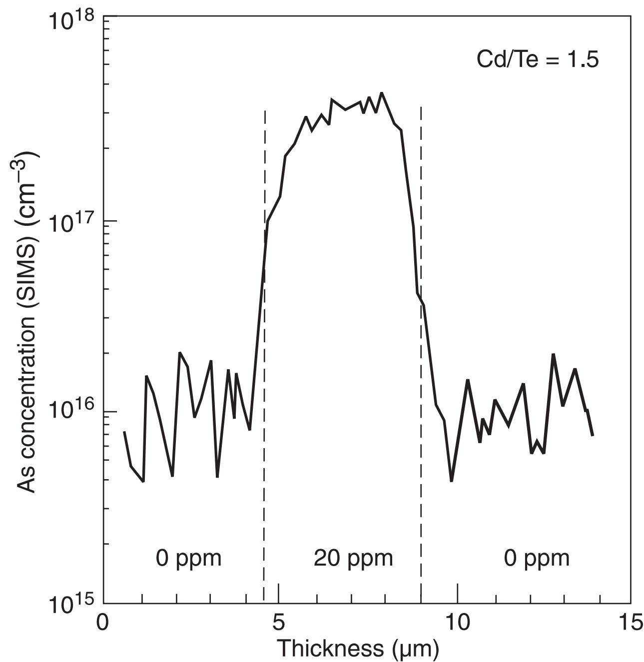

Fig. 14. SIMS concentration profile of a 4.5-μm thick test structure, doped using AsH_3 (from 0 to 4.5 μm and above 9 μm the structure was undoped). The structure was grown with Cd/Te ratio of 1.5.

off. The SIMS profile clearly showed the abrupt nature of both transitions between undoping and highly doping concentrations. It also indicates that the reactor memory was minimized.

P-type doping using AsH_3 precursor was achieved over the range of 3×10^{15}–5×10^{17} cm^{-3} in IMP growth, where the As-precursors are injected in the CdTe growth cycle under Cd-rich conditions. For example, Fig. 15 shows the hole concentration of arsenic doped (111)$Hg_{0.72}Cd_{0.28}Te$ layers at 77 K vs. arsine concentration in reactor. The HgCdTe layers were grown with Cd/Te ratio of 1.5. Thermal annealing is required to enhance activation of the As acceptors. As indicate Fig. 15, an *ex-situ* isothermal annealing in high mercury vapours (360/350°C) shows significant effects on acceptor doping by increasing the hole concentration.

It is much more difficult to achieve heavily doped x-low HgCdTe materials. Arsenic incorporates only during CdTe cycle in IMP growth process. The growth time of CdTe cycle (the active time of As doping) is considerably shorter than HgTe cycle for x-low layers. As a result, the relative arsenic incorporation is worse in epilayers with x-low compositions than in x-high ones. The investigation of optimal growth conditions for more effective doping in x-low layers is still continued. So far, after postgrowth annealing, concentrations of up to 3×10^{17} cm^{-3} have been achieved. Figure 16 shows that hole concentration of 2×10^{17} cm^{-3} in (111)$Hg_{0.83}Cd_{0.17}Te$ layer can be achieved under the following growth conditions: Cd/Te ratio equal to 5 and arsine fraction of 4 ppm in the growth zone (mercury temperature of 220°C). Higher doping concentrations (>5×10^{17} cm^{-3}) have been achieved in the higher x, postgrowth annealing materials ($x > 0.25$) with Hg temperature of 220°C and arsine fraction of 10 ppm.

Figure 17 shows the relationship between 77 K hole mobility measured at 2 kG magnetic filed strength and composition. The hole concentration at 77 K range from 10^{16}–3×10^{17} cm^{-3}. The mobility decreases with increasing CdTe mole fraction in HgCdTe alloy. We can also notice independence of mobility values on a dopant source.

Early studies of arsenic doped MOCVD HgCdTe layers using $TBAsH_2$ and $PhAsH_2$ precursors indicated that the carrier lifetimes were significantly lower than those obtained in As-doped HgCdTe grown by Hg-rich liquid phase

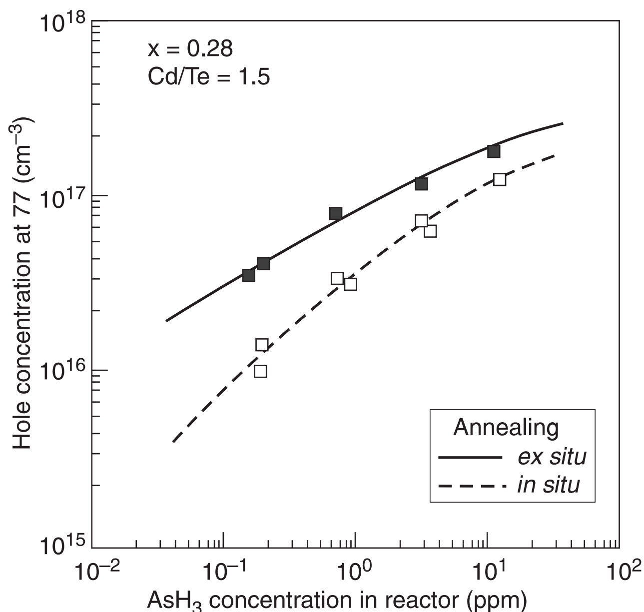

Fig. 15. 77 K hole concentration of arsenic doped (111)$Hg_{0.72}Cd_{0.28}Te$ layers vs. arsine concentration. The HgCdTe layers were grown with Cd/Te ratio of 1.5.

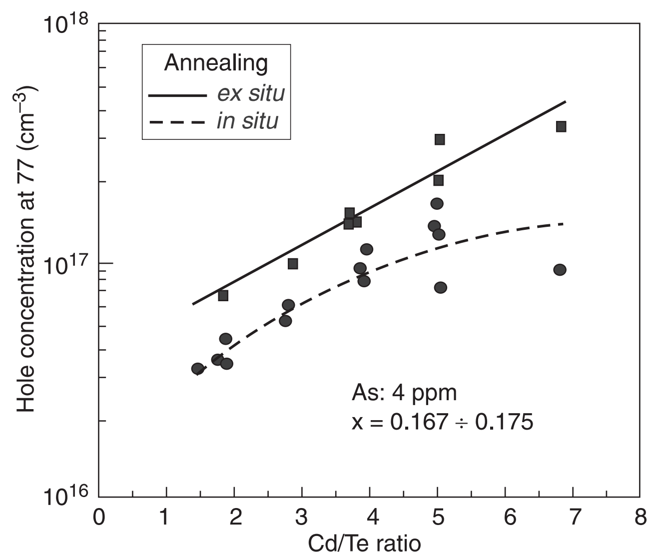

Fig. 16. Room temperature hole concentration for arsenic doped (111)$Hg_{1-x}Cd_xTe$ ($x \approx 0.17$) vs. Cd/Te ratio maintained during growth.

 © 2005 COSiW SEP, Warsaw

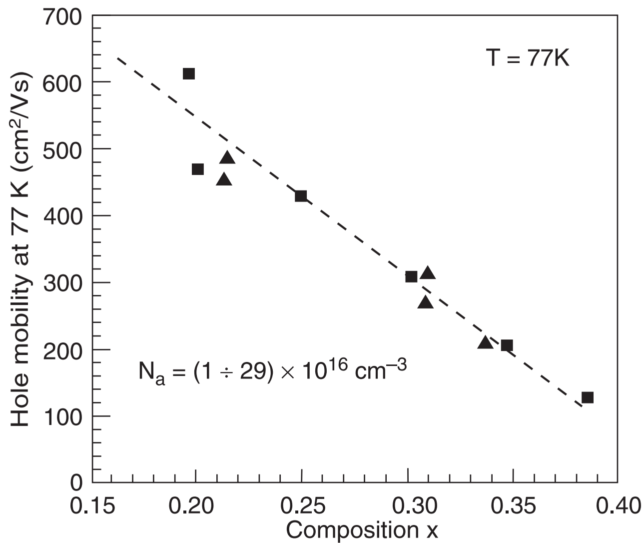

Fig. 17. 77 K hole mobility for As-doped $Hg_{1-x}Cd_xTe$ layers vs. composition. The layers have been doped using tertiarybutylarsine (■, after Ref. 27) and arsine (▲, our results). The 77 K carrier concentration for the data range from 10^{16}–3×10^{17} cm^{-3}.

epitaxy (LPE) [24,27]. It was suggested [28] that As-doping of CdTe with AsH_3 causes the incorporation of As-H pairs in addition to As. It is likely that As-H pairs are incorporated also with $TBAsH_2$ and $PhAsH_2$ precursors since they are substituted AsH_3 in MOCVD HgCdTe growth. Although As-H complexes are expected to be electrically neutral, they are likely to be recombination centres in HgCdTe and are probably an important factor in the lower lifetimes observed in As-doped films grown with the $TBAsH_2$ and $PhAsH_2$ precursors. Unlike $TBAsH_2$ and $PhAsH_2$, dimethylaminoarsenic (DMAAs) – another precursor used for p-type HgCdTe doping [9,28,29], has no As-H bonds and it is therefore expected that As-H complexes will not be incorporated in the As-doped films.

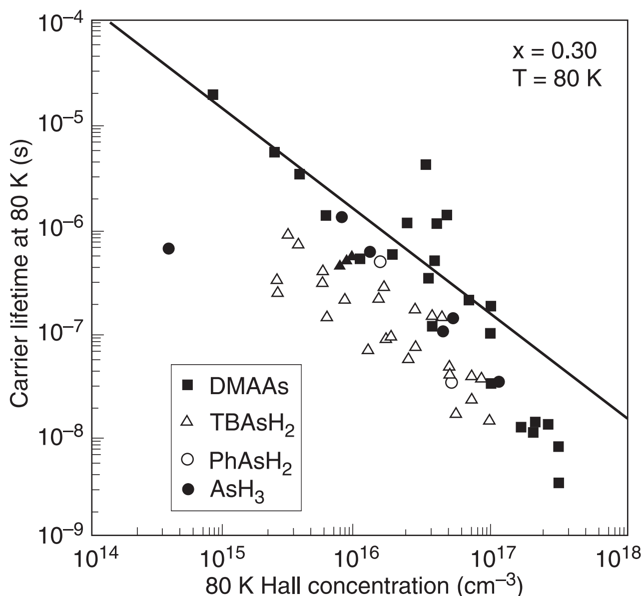

Fig. 18. Comparison of 80 K lifetimes in As-doped $Hg_{1-x}Cd_xTe$ ($x \approx 0.30$) layers from DMAAs, $TBAsH_2$, $PhAsH_2$, and AsH_3. The experimental data for HgCdTe layers grown with DMAAs, $TBAsH_2$, and $PhAsH_2$ precursors are taken from Ref. 9; our results (●) concerns HgCdTe laters doped with AsH_3. The solid line represents traditional radiative limit for $Hg_{0.70}Cd_{0.30}Te$ (without including reabsorption effects).

Figure 18 compares lifetime measurements reported for As-doped $Hg_{1-x}Cd_xTe$ ($x \approx 0.30$) films grown with DMAAs, $TBAsH_2$, $PhAsH_2$, and AsH_3 precursors. The data taken at 80 K are plotted as a function of the Hall concentration. It is clear that the lifetimes of the films doped with DMAAs show higher values of lifetimes than those measured in the films doped with $TBAsH_2$, $PhAsH_2$, and AsH_3. However, our experimental data obtained using AsH_3 precursor coincide well with theoretical predictions (solid line) for traditional radiative limit for $Hg_{0.70}Cd_{0.30}Te$ (without including reabsorption effects). These data provide confidence that the carrier lifetimes in As-doped MOCVD layers with AsH_3 precursor are close to the values reported in As-doped Hg-rich LPE grown HgCdTe. Next figure (Fig. 19) confirms this conclusion, where temperature-dependent carrier lifetime is shown for two $Hg_{0.69}Cd_{0.31}Te$ samples with hole concentrations 1.1×10^{16} cm^{-3} and 4.1×10^{16} cm^{-3}. Both sets of data agree well with a theoretical model that includes Auger 7 and radiative recombination mechanisms [3].

6. Conclusions

Practical implementation of the advanced photodetector architecture requires well established epitaxial technology. The paper presents recent progress in the MOCVD growth of HgCdTe epilayers on GaAs/CdTe substrates. This technique has been selected for its inherent versatility (low

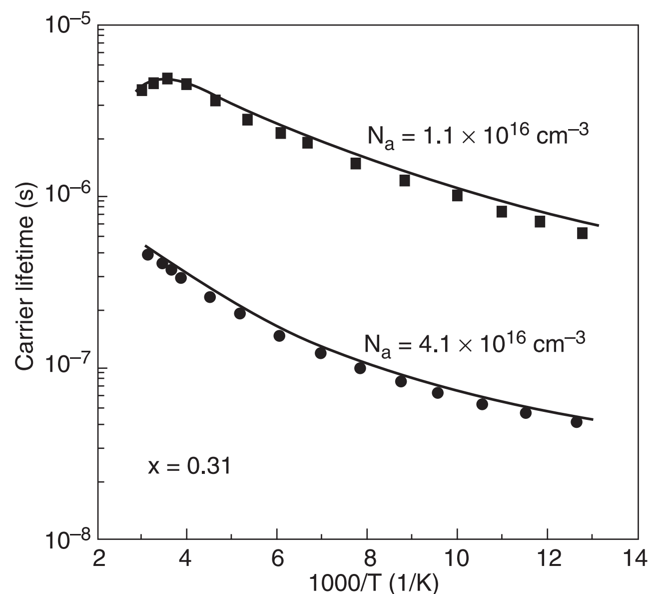

Fig. 19. Temperature dependence of lifetimes measured for $Hg_{0.69}Cd_{0.31}Te$ samples with hole concentrations 1.1×10^{16} cm^{-3} and 4.1×10^{16} cm^{-3} and comparison to the theoretical model (solid lines).

growth temperature, ability to grow layered structures with complex composition and doping profiles while maintaining sharp interfaces). MOCVD makes possible to use low-cost and high quality substrates (GaAs, sapphire and silicon) and has the potential for a large-scale cost-effective production.

HgCdTe heterostructures have been grown on 2'' (100)GaAs. Reproducible n- and p-type doping at the low, intermediate and high level (10^{15}–10^{18} cm^{-3}) has been achieved with stable iodine and arsenic dopants. The dopants are easily activated during growth. Sharp iodine profiles have been obtained without any memory effects, a key requirements for bandgap engineering HgCdTe devices. Also SIMS profiles of arsenic doped heterostructures indicate that the reactor memory was minimized. The doping range especially meets the requirements for HgCdTe photovolataic devices operated at near room temperatures in both MW and LW infrared spectral ranges [30].

The transport properties of MOCVD layers are comparable with those published for LPE epilayers. The experimental data provide confidence that the carrier lifetimes in MOCVD layers are close to theoretical limits determined by radiative and Auger recombinations.

Acknowledgments

This work was supported by the Polish Ministry of Science and Information Technology in the frame of the project No. PBZ-MIN-009/T11/2003.

References

1. W.D. Lawson, S. Nielson, E.H. Putley, and A.S. Young, "Preparation and properties of HgTe and mixed crystals of HgTe-CdTe", *J. Phys. Chem. Solids* **9**, 325–329 (1959).
2. P. Capper, "Bulk growth techniques", in *Narrow-gap II-VI Compounds for Optoelectronic and Electromagnetic Applications,* pp. 3–29, edited by P. Capper, Chapman & Hall, London, 1997.
3. A. Rogalski, K. Adamiec, and J. Rutkowski, *Narrow-Gap Semiconductor Photodiodes,* SPIE Press, Bellingham, 2000.
4. P. Norton, "HgCdTe infrared detectors", *Opto-Electron. Rev.* **10**, 159–174 (2002).
5. L. Colombo, R.R. Chang, C.J. Chang, and B.A. Baird, "Growth of Hg-based alloys by the travelling heater method", *J. Vac. Sci. Technol.* **A6**, 2795–2799 (1988).
6. P. Capper, T. Tung, and L. Colombo, "Liquid phase epitaxy", in *Narrow-gap II-VI Compounds for Optoelectronic and Electromagnetic Applications,* pp. 30–170, edited by P. Capper, Chapman & Hall, London, 1997.
7. S.J.C. Irvine, "Metal-organic vapour phase epitaxy", *Narrow-gap II-VI Compounds for Optoelectronic and Electromagnetic Applications*, pp. 71–96, edited by P. Capper, Chapman & Hall, London, 1997.
8. O.K. Wu, T.J. deLyon, R.D. Rajavel, and J.E. Jensen, "Molecular beam epitaxy of HgCdTe", in *Narrow-gap II-VI Compounds for Optoelectronic and Electromagnetic Applications,* pp. 97–130, edited by P. Capper, Chapman & Hall, London, 1997.
9. P. Mitra, F.C. Case, and M.B. Reine, "Progress in MOVPE of HgCdTe for advanced infrared detectors", *J. Electron. Mater.* **27**, 510–520 (1998).
10. M.B. Reine, A. Hairston, P. O'Dette, S.P. Tobin, F.T. J. Smith, B L. Musicant, P. Mitra, F.C. Case, "Simultaneous MW/LW dual-band MOCVD HgCdTe 64×64 FPAs", *Proc. SPIE* **3379**, 200–212 (1998).
11. C.D. Maxey, J.P. Camplin, I.T. Guilfoy, J. Gardner, R.A. Lockett, C.L. Jones, P. Capper, M. Houlton, and N.T. Gordon, "Metal-organic vapour-phase epitaxial growth of HgCdTe device heterostructures on three-inch-diameter substrates", *J. Electron. Mater.* **32**, 656–660 (2003).
12. C.T. Elliott, "New infrared and other applications of narrow gap semiconductors", *Proc. SPIE* **3436**, 763–775 (1998).
13. C.T. Elliott, "Photoconductive and non-equilibrium devices in HgCdTe and related alloys", in *Infrared Detectors and Emitters: Materials and Devices*, pp. 279–312, edited by P. Capper and C.T. Elliott, Kluwer Academic Publishers, 2001.
14. J. Piotrowski, W. Galus, and M. Grudzień, "Near room-temperature IR photodetectors," *Infrared Phys.* **31**, 1–48 (1991).
15. J. Piotrowski, Z. Nowak, J. Antoszewski, C. Musca, J. Dell, and L. Faraone, "A novel multi-heterojunction HgCdTe long-wavelength infrared photovoltaic detector for operation under reduced cooling conditions", *Semicond. Sci. Technol.* **13**, 1209–1214 (1998).
16. J. Piotrowski, "Uncooled operation of IR photodetectors", *Opto-Electron. Rev.* **12**, 111–122 (2004).
17. W.E. Tennant, C.A. Cockrum, J.B. Gilpin, M.A. Kinch, M. B. Reine, R.P. Ruth "Key issues in HgCdTe-based focal plane arrays: An industry perspective" *J. Vac. Sci. Technol.* **B10**, 1359–1369(1992).
18. L.M. Smith and J. Thompson, "Metal organic chemical vapour deposition (MOCVD) of cadmium telluride, mercury telluride and cadmium mercury telluride", *Chemtronics* **4**, 60–70 (1989).
19. S.A. Svoronos, W.W Woo, S.J.C. Irvine, H.O. Sankur, and J. Bajaj, "A model of the interdiffused multilayer process", *J. Electron. Mater.* **25**, 1561–1571 (1996).
20. C. Theodoropoulos, N.K. Ingle, and T.J. Mountziaris, "Computational studies of the transient behaviour of horizontal MOVPE reactors", *J. Cryst. Growth* **170**, 72–76 (1997).
21. H.R. Vydyanath, "Donor and acceptor dopants in $Hg_{1-x}Cd_xTe$ alloys", *J. Vac. Sci. Technol.* **B9**, 1716–1723 (1991).
22. P. Mitra, Y.L. Tyan, T.R. Schimert, and F.C. Case, "Donor doping in metalorganic chemical vapour deposition of HgCdTe using ethyl iodine", *Appl. Phys. Lett.* **65**, 195–197 (1994).
23. P. Mitra, F.C. Case, M.B. Reine, R. Starr, and M.H. Weiler, "Doping in MOVPE of HgCdTe: orientation effects and growth of high performance IR photodiodes", *J. Cryst. Growth* **170**, 542–548 (1997).
24. C.D. Maxey, I.G. Gale, J.B. Clegg, and P.A.C. Whiffin, "Doping studies in MOVPE-grown $Cd_xHg_{1-x}Te$", *Semicond. Sci. Technol.* **8**, S183–S196 (1993).
25. L. Svob, I. Cheze, A. Lusson, D. Ballutaud, J.F. Rommeluere, and Y. Marfaing, "Crystallographic orientation dependence of As incorporation in MOVPE-grown CdTe and corresponding acceptor electrical state activation", *J. Cryst. Growth* **184/185**, 459–464 (1998).
26. S.J.C. Irvine, J. Bajaj, L.O. Bubulac, W.P. Lin, R.W. Gedridge, and K.T. Higa, "A new n-type doping precursor

 © 2005 COSiW SEP, Warsaw

for MOCVD-IMP growth of detector quality MCT", *J. Electron. Mater.* **22**, 859–864 (1993).

27. D.D. Edwall, L.O. Bubulac, and E.R. Gertner, "p-type doping of metalorganic chemical vapour deposition-grown HgCdTe by arsenic and antimony", *J. Vac. Sci. Technol.* **B10**, 1423–1427 (1992).
28. M.J. Bevan, M.C. Chen, and H.D. Shih, "High-quality p-type $Hg_{1-x}Cd_xTe$ prepared by metalorganic chemical vapour deposition", *Appl. Phys. Lett.* **67**, 3750–3752 (1995).
29. P. Mitra, Y.L. Tyan, F.C. Case, R. Starr, and M.B. Reine, "Improved arsenic doping in metalorganic chemical vapour deposition of HgCdTe and *in-situ* growth of high performance long wavelength infrared photodiodes", *J. Electron. Mater.* **25**, 1328–1335 (1996).
30. J. Piotrowski and A. Rogalski, "Uncooled long wavelength infrared photon detectors", *Infrared Phys. Technol.* **46**, 115–131 (2004).

Semiconductor Device Technology

from Cambridge University Press

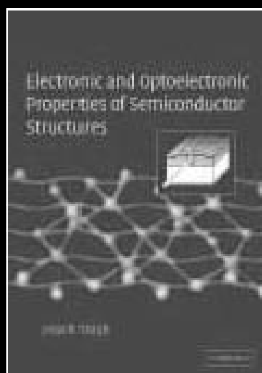

Electronic and Optoelectronic Properties of Semiconductor Structures

Jasprit Singh
University of Michigan, Ann Arbor, USA

Presenting the underlying physics behind devices that drive today's technologies. The book covers important details of structural properties, bandstructure, transport, optical and magnetic properties of semiconductor structures. Effects of low-dimensional physics and strain – two important driving forces in modern device technology – are also discussed. In addition to conventional semiconductor physics the book discusses self-assembled structures, mesoscopic structures and the developing field of spintronics. The book utilizes carefully chosen solved examples to convey important concepts and has over 250 figures and 200 homework exercises. Real-world applications are highlighted throughout the book, stressing the links between physical principles and actual devices. Electronic and Optoelectronic Properties of Semiconductor Structures provides engineering and physics students and practitioners with complete and coherent coverage of key modern semiconductor concepts. A solutions manual and set of viewgraphs for use in lectures are available for instructors, from solutions@cambridge.org.

Features

- *Detailed and up-to-date coverage of the latest semiconductor devices, linking theoretical concepts with real-world applications*
- *Includes numerous worked examples and homework exercises*

Contents: Preface; Introduction; 1. Structural properties of semiconductors; 2. Semiconductor bandstructure; 3. Bandstructure modifications; 4. Transport: general formalism; 5. Defect and carrier-carrier scattering; 6. Lattice vibrations: phonon scattering; 7. Velocity-field relations in semiconductors; 8. Coherence, disorder, and mesoscopic systems; 9. Optical properties of semiconductors; 10. Excitonic effects and modulation of optical properties; 11. Semiconductors in magnetic fields; Appendices.

2003 554pp 288 Illustrations 199 exercises
0 521 82379 X Hardback £37.50

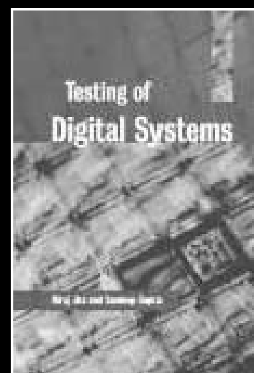

Testing of Digital Systems

Niraj Jha
Princeton University, New Jersey, USA

Sandeep Gupta
University of Southern California, USA

Device testing represents the single largest manufacturing expense in the semiconductor industry, costing over US $40 billion a year. The most comprehensive and wide ranging book of its kind, Testing of Digital Systems covers everything you need to know about this vitally important subject. Starting right from the basics, the authors take the reader through automatic test pattern generation, design for testability and built-in self-test of digital circuits before moving on to more advanced topics such as IDDQ testing, functional testing, delay fault testing, memory testing, and fault diagnosis. The book includes detailed treatment of the latest techniques including test generation for various fault modes, discussion of testing techniques at different levels of integrated circuit hierarchy and a chapter on system-on-a-chip test synthesis.

Features

- *Most comprehensive book yet on digital systems testing*
- *Covers all the latest techniques*
- *Includes System-on-a-Chip testing*

Contents: 1. Introduction; 2. Fault models; 3. Combinational logic and fault simulation; 4. Test generation for combinational circuits; 5. Sequential ATPG; 6. IDDQ testing; 7. Functional testing; 8. Delay fault testing; 9. CMOS testing; 10. Fault diagnosis; 11. Design for testability; 12. Built-in self-test; 13. Synthesis for testability; 14. Memory testing; 15. High-level test synthesis; 16. System-on-a-chip testing; Index.

2003 1016pp 559 illustrations
0 521 77356 3 Hardback £65.00

CAMBRIDGE
UNIVERSITY PRESS